

---

# TOWARDS PHYSICALLY INTERPRETABLE WORLD MODELS: MEANINGFUL WEAKLY SUPERVISED REPRESENTATIONS FOR VISUAL TRAJECTORY PREDICTION

---

**Zhenjiang Mao**

Department of Electrical and Computer Engineering  
University of Florida  
Gainesville, FL  
z.mao@ufl.edu

**Ivan Ruchkin**

Department of Electrical and Computer Engineering  
University of Florida  
Gainesville, FL  
iruchkin@ece.ufl.edu

## ABSTRACT

Deep learning models are increasingly employed for perception, prediction, and control in complex systems. Embedding physical knowledge into these models is crucial for achieving realistic and consistent outputs, a challenge often addressed by physics-informed machine learning. However, integrating physical knowledge with representation learning becomes difficult when dealing with high-dimensional observation data, such as images, particularly under conditions of incomplete or imprecise state information. To address this, we propose Physically Interpretable World Models, a novel architecture that aligns learned latent representations with real-world physical quantities. Our method combines a variational autoencoder with a dynamical model that incorporates unknown system parameters, enabling the discovery of physically meaningful representations. By employing weak supervision with interval-based constraints, our approach eliminates the reliance on ground-truth physical annotations. Experimental results demonstrate that our method improves the quality of learned representations while achieving accurate predictions of future states, advancing the field of representation learning in dynamic systems.

## 1 Introduction

Autonomous systems operating in dynamic environments, such as robots and autonomous vehicles, increasingly require accurate and robust trajectory prediction to ensure safe and efficient operation. Deep learning models, such as Long Short-Term Memory (LSTM) [1] networks and Gated Recurrent Units (GRUs) [2], have shown considerable success in state prediction by capturing temporal dependencies effectively from raw data. Furthermore, physics-informed models, like Physics-Informed Neural Networks (PINNs) [3] and Neural Ordinary Differential Equations (Neural ODEs) [4], integrate physical dynamics into the learning process, thus bridging the gap between data-driven learning and first-principles knowledge. However, in real-world applications, internal physical states are often not fully accessible; some may only be partially observable, while others may be completely hidden. This limitation leaves only high-dimensional observations, such as images and lidar scans, as indirect sources of information on critically important properties like position or safety. Complicating matters further, the underlying dynamical systems are not fully known, making physics-informed approaches difficult to apply.

Given these challenges, recent research has shifted focus to the prediction of *observations* as a way to gain insights into the system's behavior. Models such as convolutional LSTMs [5] can predict sequences of observations, but due to the high dimensionality of the data and the resulting network complexity, their performance is often limited. Although the convolutional LSTM [5] has hidden layers to extract relevant features, it is difficult to maintain global consistency of these features across the entire sequence without systematic learning. To address this issue, many approaches have turned to learning *latent representations* to reduce dimensionality and extract useful features. For instance, Variational Autoencoders (VAEs) [6] have proven particularly effective for this purpose, as they offer an unsupervised way to learn compact latent spaces while enabling the reconstruction of high-dimensional observations. World models [7] build on VAEs and integrate predictive components such as mixed-density Recurrent Neural Networks (RNNs) to capture

temporal dependencies and enable accurate predictions of future actions in image-based controllers, which can be used for safety monitoring of learning-enabled autonomous systems [8]. Recent advancements [9] leverage these combined structures to enhance both predictive accuracy and generative performance, particularly in complex and highly uncertain environments.

Despite these advantages, the representations learned by these models remain abstract numbers with limited if any physical meaning, making it challenging to relate them directly to the system’s true internal states. Connecting these representations to the system’s true internal states would enhance the interpretability and trustworthiness of the predictions as well as the long-term controllability of the CPS, especially in complex and high-risk scenarios. For example, in an autonomous driving system, linking latent representations to the vehicle’s physical states allows the model to generate causal explanations for decisions (such as slowing down due to occlusions). Doing so would also enable the application of high-assurance methods, such as formal verification [10] and run-time shielding [11], to end-to-end learning pipelines. A promising step in this direction is causal VAEs [12], which not only create meaningful representations but also learn causal relationships between variables, providing a more structured understanding of the system’s dynamics. Unfortunately, they depend on exact supervision labels, which are often difficult to obtain due to the limited budget, time, and expertise.

This paper targets a prediction setting without the *exact supervision of physical labels*, with only weak supervisory signals to guide learned representations toward physical meaning. Such signals are often overlooked but can be encoded as valuable constraints, such as the fact that a car’s speed is unlikely to exceed 350 km/h. We represent these constraints as intervals and propose to use them as weak supervision in representation learning to encode high-dimensional images into physically interpretable representations. Once the learned representation possesses physical meaning, it can be combined with the jointly learned dynamical system to predict future states. This capability is a step along the pathway to robust state prediction and decision-making in complex systems.

The central goal of this paper is to design and train *Physically Interpretable World Models* (PIWMs) by incorporating dynamics as a learnable component within the prediction pipeline and applying weak supervision to physical states.

By leveraging dynamical equations as a structural foundation that integrates latent representations as inputs, and applying weak supervision directly to the representations, we hypothesize that PIWMs will improve the capability to learn representations that accurately reflect the system’s true physical state. Thus, our research addresses two key questions: (1) How effectively can a physically meaningful representation be learned from weak supervision? (2) To what extent can these learned representations predict future physical states?

Based on the results of two case studies — cart pole and lunar lander — we demonstrate that our model can learn representations closely aligned with actual physical states and perform well in forward prediction tasks. This indicates that integrating dynamics and weak supervision contributes positively to both the interpretability and predictive accuracy of the learned representations. The contributions of our work are summarized below:

- A novel learning architecture designed to encode physically meaningful representations from high-dimensional observations in closed-loop systems.
- A training pipeline that effectively incorporates weak supervision and accommodates unknown dynamics.
- Experimental results demonstrate superior performance in both physical interpretability and predictive accuracy compared to traditional world models.

The next section provides an overview of existing research. Section 3 introduces the background and formulates the problem we aim to address. Section 4 describes our proposed learning architecture and training methodology. Section 5 presents two case studies and the experimental results. Finally, Section 6 concludes with a brief discussion.

## 2 Related Work

### 2.1 Learning Latent Representations

Latent representations are essential for neural networks to capture the underlying structure of complex data by encoding it into low-dimensional spaces. This way of reducing data dimensionality helps models distill key features from high-dimensional data such as images, texts, and audio, while discarding redundant or unimportant information. Learning effective latent representations has proven useful in tasks like image generation [13], data compression [14], clustering [15], classification [16], anomaly detection [17, 18] and style transfer [19]. Variational Autoencoders (VAEs) [6] are widely used in this context, with an encoder that compresses input data into a compact latent space and a decoder that reconstructs the original input from this space. However, the vanilla VAE is not suitable for learning

representations with physical meaning, as it does not explicitly encourage the latent space to capture interpretable or structured features.

To make latent representations more interpretable,  $\beta$ -VAE [20] introduces a hyperparameter  $\beta$  to disentangle the latent space, encouraging each dimension of the latent vector to capture independent features. Despite this improvement,  $\beta$ -VAE representations usually lack physical interpretability: the learned features cannot be directly linked to real-world physical states. Other studies, such as those involving neural state variables [21], aim to learn representations closely related to physical states by employing geometric manifold learning techniques (e.g., the Levina-Bickel algorithm) to analyze the geometric structure of the autoencoder’s latent space. Manifold learning estimates the number of independent variables in the latent space based on neighborhood distances, ensuring the extracted variables align with the system’s physical complexity, thereby maintaining a strong correlation with physical states. CausalVAE [12, 22] takes a further step toward interpretability by enforcing causal relationships within the latent space using a causal graph. However, these models heavily depend on strong supervision with labeled causal states, which is impractical in most applications. However, our approach does not aim to achieve an optimal representation of these rules; instead, we prioritize improving task-specific outcomes. Our approach relaxes this need by using weak supervision signals to guide the learning of physically meaningful representations. Other models like banana [23] incorporate task-related domain rules into the prior distribution of Bayesian neural networks to enhance the model’s performance, reliability, and uncertainty quantification in classification or regression tasks.

Other researchers attempt to extract useful information from high-dimensional data through the process of abstraction [24, 25, 26]. Abstracted valuable information can be utilized for policy learning with higher efficiency, as it highlights the core motion information of an object or point while excluding redundant visual details [27]. Abstraction techniques, while effective, often require supervised labels [28] or external subjective guidance, such as human language [29, 30]. Abstraction typically aims to create simplified, high-level representations, but these representations are difficult to map back to the original high-dimensional data, limiting their applications with the need for interoperability.

## 2.2 Dynamics-Based Learning

In planning and decision-making tasks, learned dynamics are often implemented with neural networks to capture how observations evolve with different actions, as seen in world models like Dreamer [31, 32, 33]. These world models create simulated “worlds” that allow for policy learning without real-world trial-and-error costs. However, due to reliance on commonplace deep learning pipelines, such models often lack interpretable latent representations, and their performance is constrained by the quality and quantity of training samples. When the data-driven learned prediction module is faced with unseen or out-of-distribution data, its performance degrades due to limited generalization.

To improve prediction fidelity and ensure that world models align with physical realities, researchers have incorporated physical constraints on control inputs, such as acceleration and steering angles, limiting them to a physical system’s actual operational limits [34]. Embedding motion equations directly into neural networks, for example, as kinetic layers [35], allows the model to predict trajectories at the state level (e.g., position and speed) that respect real-world physics. However, these strict physics-based constraints require accurate physical data, and when such data is noisy or partially known, prediction errors tend to increase. Alternative approaches introduce other types of constraints — such as temporal logic [36] and social pooling [37, 38, 39] — to shape model outputs, particularly in low-dimensional scenarios. Though effective, these methods often face limitations in handling high-dimensional observations, and the latent representations they generate are frequently less interpretable when applied to more complex systems.

Additionally, value-based constraints seek to confine neural network outputs within ranges specified by physical laws [40], while some approaches incorporate prior physical knowledge as loss functions during training [41]. Both methods have seen successful applications but focus on low-dimensional state inputs. For scenarios involving limited or noisy sensor data, physics-informed VAEs [42] are designed to leverage physical laws, such as stochastic differential equations (SDEs), to stabilize learning under uncertainty. Despite these advances, obtaining fully interpretable latent representations remains challenging, especially in high-dimensional settings with partial information.

Our approach builds on the above literature by incorporating physical dynamics into its architecture; moreover, it contrasts with existing methods by relying only on weak supervision signals in the form of real-valued intervals, thus overcoming the need for precise physical labels.

## 2.3 Trajectory Prediction

A trajectory is a temporal sequence of states or observations. Predicting trajectories plays a crucial role in enabling autonomous CPS to anticipate and avoid dangers, such as vehicle collisions [43]. By forecasting the behavior of surrounding agents, trajectory prediction provides vital information for planning and control [44].

Traditional model-based approaches, such as Kalman filtering [43] and Hamilton-Jacobi (HJ) reachability [45, 46], provide safety guarantees based on explicit dynamical models. These methods enable precise risk estimation but require detailed knowledge of system dynamics and are computationally intensive, making them inapplicable in high-dimensional and complex environments.

With the advent of deep learning, predictors have become more flexible in handling complexity. World models, for instance, can also be a trajectory predictor that integrates autoencoders with recurrent modules like Recurrent Neural Networks (RNNs) in an encoding-predicting-decoding structure [7, 9]. This structure simulates diverse scenarios within a physical world, enhancing the model’s capacity to predict trajectories from images and quantify uncertainty in long-horizon forecasts [47]. Such composite architectures typically outperform simpler networks, such as Convolutional-LSTM [5], in trajectory and safety prediction [47, 8]. Trajectron++[48] further extends this capability by integrating scene graphs with conditional VAEs to forecast multi-agent trajectories, though it still relies heavily on handcrafted scene representations. Recent advancements, such as confidence-aware prediction methods, help assess model reliability in real-time applications [44, 49]. Further enhancing reliability, conformal prediction can provide statistically valid uncertainty intervals around deep learning predictors [50, 51], though it is orthogonal to physical interpretability and requires the exact ground truth. [52] Explainable predictions like the Interpretable Self-Aware Prediction (ISAP) framework utilize input divided into three semantic components: the vehicle’s historical trajectory, high-precision maps, and encodings of trajectories from surrounding vehicles or pedestrians. Human-like responsibility metrics are introduced to latent variables, enabling the integration of discrete behavior abstractions and the use of reward-based frameworks to provide clear causal explanations for model outputs. Human-like responsibility metrics [53] are introduced to trajectory prediction, enabling the integration of discrete behavior abstractions and the use of reward-based frameworks to provide clear causal explanations for model outputs. These metrics guide the model to predict trajectories that align with human values, such as avoiding unsafe overtaking maneuvers. However, no interpretable learning is applied at the representation level. In contrast, our approach bypasses the need for handcrafted representations by directly learning from images and interval-based labels.

### 3 Problem Formulation

#### 3.1 Dynamical System and Sequence Prediction

**Definition 1 (Dynamical System)** *A dynamical system  $s = (X, A, \phi_\psi, g, I)$  describes the state evolution of an image-controller system with any image-based controller  $h$ :*

- State set  $X$ : finite-dimensional and containing states  $x$
- Action set  $A$
- Dynamics function  $\phi$  (with parameters  $\psi$ ):  $X \times A \times \Psi \rightarrow X$
- Observation function  $g$ :  $X \rightarrow Y$
- Initial state set  $I$
- Controller  $h$ :  $Y \rightarrow A$

The states of the system evolve as:

$$x_{t+1} = \phi_\psi(x_t, a_t). \quad (1)$$

If we define a scalar output function  $R(x_1, \dots, x_T)$  (for instance, based on the final state  $x_T$  or the entire state trajectory), the gradient with respect to  $\psi$  can be derived using the chain rule. For the final state  $x_T$ , we have:

$$\frac{\partial R}{\partial \psi} = \frac{\partial R}{\partial x_T} \cdot \frac{\partial x_T}{\partial \psi}. \quad (2)$$

Since  $x_T$  depends on all previous states and parameters, we can expand this as:

$$\frac{\partial x_T}{\partial \psi} = \frac{\partial \phi_\psi(x_{T-1}, a_{T-1})}{\partial \psi} + \frac{\partial \phi_\psi(x_{T-1}, a_{T-1})}{\partial x_{T-1}} \frac{\partial x_{T-1}}{\partial \psi}. \quad (3)$$

By recursively applying this relationship, we express the final gradient in terms of a product (and sum) of Jacobians and gradients of  $\phi_\psi$  with respect to its inputs and parameters.

Such systems usually rely on observations  $y$  generated by sensors given any observation-based controllers. We assume that the controller  $h$  is known, as we are monitoring the controlled system and can observe its behavior. These controllers are usually trained by imitation learning [54] or reinforcement learning [55] like deep Q-networks [56] and deep deterministic policy gradient (DDPG) [57]. An RGB camera takes a picture  $y_t$  at time  $t$ , which contains information about  $x_t$  and is used for control.

Given an initial state  $x_0 \in I$  and a sequence of actions  $a_{0:i}$ , the state trajectory of the system is defined by iteratively applying the dynamic function  $\phi$ , yielding a sequence  $(x_0, x_1, \dots, x_{i+1})$ , where each state is  $x_{t+1} = \phi(x_t, a_t)$ . Correspondingly, the observation trajectory  $(y_0, y_1, \dots, y_{t+1})$  is generated by applying the observation function  $g$  to each state, where  $y_t = g(x_t)$ .

Since dynamical systems evolve over time, forecasting future observations provides the foundation for understanding system behavior and enabling autonomous systems to perform downstream tasks. For example, detecting potentially dangerous objects allows the system to adjust its controller to improve avoidance or switch to a safety-oriented meta-policy to ensure safe operation. These downstream tasks often involve computer vision functions, such as classification, object detection, or semantic segmentation.

**Definition 2 (Observation Prediction)** A sequence predictor  $f_{pred}$  at time  $t$  takes a sequence  $y_{t-m:t}$  of images with length  $m$  as input and predicts images for the next  $n$  steps:  $y_{t+1:t+n}$ .

- Prediction vector:  $\hat{y}_{(t+1:t+n)} = f_{pred_o}(y_{t-m:t})$

Achieving high-quality predictions is critical, as the effectiveness of downstream tasks depends on the accuracy of predicted images. However, since images are high-dimensional data, existing discriminative models like convolutional neural networks (CNNs) often struggle to deliver sufficient prediction quality. This challenge motivates the use of dimensionality-reducing methods centered on predicting *latent representations*.

Since the image-controlled system ultimately requires high dimensional observations to generate actions and predict future states, a decoder structure, which can reconstruct the low-dimensional data back to the original image domain, becomes essential. To address this, the Variational Autoencoder (VAE) [6], an unsupervised generative model, offers a solution. By using a CNN-based encoder and deconvolutional layers as the decoder, the VAE can reconstruct the latent representation back into high-dimensional space, restoring it to a form suitable for task-specific processing and interpretation (e.g., an image). This reconstruction capability allows downstream tasks to leverage both the efficiency of lower-dimensional representations and the richness of high-dimensional data.

**Definition 3 (Latent Sequence Prediction)** An encoder  $f_{enc}$  compresses the high-dimensional observation input  $y$  into a latent representation  $z$  and a predictor  $f_{pred}$  predicts the future latent representations. A decoder  $f_{dec}$  to transform the latent representation back to the observation space:

- Encoding:  $z_{t-m:t} = f_{enc}(y_{t-m:t})$
- Prediction:  $z_{t+1:t+n} = f_{pred_z}(z_{t-m:t})$
- Decoding  $\hat{y}_{t+1:t+n} = f_{dec}(z_{t+1:t+n})$

Our primary use case is predicting the behavior of a learning-enabled system, where the future state depends on both the current state and the action taken by the controller. When the prediction model does not explicitly incorporate actions, it inherently learns the behavior of the controller from the training data. This approach limits the model’s generalizability, as it becomes tied to the specific controller used during training. To enable the model to generalize across different controllers, we include the action  $a$  as additional input alongside the observation or latent representation. By explicitly modeling the influence of actions, the predictor can better account for how different actions lead to different outcomes, making it more adaptable to varied controllers. Therefore, we will include the action as an input along with the observation or latent representation, thus pairing the action  $a$  generated by the controller  $h$  based on the image  $y$  with either images  $(y, a)$  or latent vectors  $(z, a)$  to make predictions. In this way, the predictor functions like a dynamical system, taking both action and current representation as inputs to predict future states as a surrogate model of the dynamics:

$$y_{t+1} = f_{pred_o}(y_t, a_t) \text{ or } z_{t+1} = f_{pred_z}(z_t, a_t). \quad (4)$$

### 3.2 Physical Representation Learning and Prediction with Weak Supervision

Although true physical states cannot be measured precisely, it is often possible to obtain a reasonable range (in some cases, based on a probability distribution) for these states based on high-dimensional observations. For instance, the

position may be inferred from imprecise image observations or estimated within a predefined range, which can serve as a weak supervisory signal.

In our setting, we assume that the dynamics function of the system  $\phi$  is known in its general form, such as the structure of kinematic equations. However, we do not have access to the true parameters  $\psi$ , such as the exact mass or traction coefficients, which makes the system only partially specified.

We are also given a dataset of trajectories  $V$ , consisting of  $N$  sequences of length  $M$ , where each sequence contains tuples of images, actions, and state interval labels:

$$V = \left\{ \left( y_{1:M}, a_{1:M}, [x_{1:M}^{\text{lo}}, x_{1:M}^{\text{up}}] \right)_{1:N} \right\}. \quad (5)$$

The state intervals  $[x^{\text{lo}}, x^{\text{up}}]$  were derived from the trajectories as weak supervision signals. These intervals are typically very large, spanning 2.5%, 5%, or even 10% of the entire state space, indicating highly imprecise information about the states. Such coarse state information is often available in real-world scenarios, for instance, as the approximate location or general area of an object.

Now we face two interrelated objectives: to learn a physically interpretable representation of the state and to predict the future sequence of these states and observations. The test dataset  $V'$  only contains observations that are generated from the initial state set:  $V' = f_{\text{obs}}(I)$ . All training and test data are collected and split randomly.

The representation learning problem aims to derive an internal representation  $z$  that approximates the system’s true physical states  $x$  as closely as possible. To evaluate the quality of this representation, we use the mean absolute error (**MAE**) metric. Given a sample initial observation  $y$  from the test dataset  $V'$ , we compute the corresponding interpretable latent representation  $z$ . The (**MAE**) is defined as:

$$\text{MAE}(z, x) = \|z - x\|_1, \quad (6)$$

where  $x$  is the true state and  $z$  is the learned state representation. The smaller the MAE, the better our representation aligns with the true physical state.

**Definition 4 (Representation Learning Problem)** *Given training dataset  $V$ , dynamics function  $\phi$  with unknown parameters, and controller  $h$ , the objective is to learn a state representation  $z = f_{\text{enc}}(y)$  that minimizes the distance to the true physical state  $x$ :*

$$\min_{f_{\text{enc}}} \|x - f_{\text{enc}}(y)\|_1 \quad (7)$$

The prediction problem aims to forecast future observations and state representations using past observations, actions, and constraints. This problem emphasizes the role of structured representation in providing reliable predictions of future behavior.

**Definition 5 (Prediction Problem with Meaningful Representation)** *Given a training dataset  $V$ , dynamics function  $\phi$  with unknown parameters, and controller  $h$ , the objective is to predict from observation  $y_t$  the future observation  $y_{t+k}$  and a physically meaningful state representation  $z_{t+k}$  at time  $t + k$  that minimizes two errors:*

1. *Observation prediction error:*

$$\min \|y_{t+k} - \hat{y}_{t+k}\|_2^2 \quad (8)$$

2. *State prediction error:*

$$\min \|x_{t+k} - z_{t+k}\|_1, \quad (9)$$

where  $\hat{y}_{t+k}^i$  is the predicted observation at time  $t + k$  predicted from the  $i$ -th sequence of the dataset  $V$ ,  $y_{t+k}^i$  is the true observation, and  $z_{t+k}^i$  is the predicted state representation aligned with the true physical state  $x_{t+k}^i$ .

To comprehensively evaluate the quality of the predicted observations, we use both Mean Squared Error (**MSE**) and Structural Similarity Index (**SSIM**) metrics. MSE measures the average pixel-wise error, offering a straightforward quantitative assessment of overall accuracy. However, it does not account for perceptual quality or structural integrity, which are crucial for visual consistency. SSIM, on the other hand, captures structural similarity by considering luminance, contrast, and covariance, making it more similar to human perception of image quality. By combining these metrics, we ensure both numerical accuracy and perceptual fidelity in evaluating the alignment between the predicted and true observations.

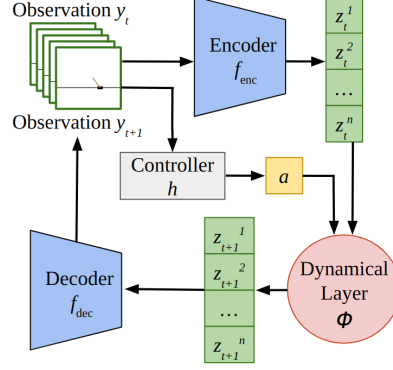


Figure 1: The architecture of our physically interpretable world models.

The MSE metric is defined as:

$$\text{MSE}(y, \hat{y}) = \frac{1}{n} \sum_{i=1}^D (y[i] - \hat{y}[i])^2 \quad (10)$$

where  $D$  represents the total number of pixels in the image  $y$ , which is typically much larger than the size of the latent representation  $d$ , corresponding to the state dimension.  $y[i]$  represents the value of the  $i$ -th pixel in  $y$ .

The SSIM metric is defined as:

$$\text{SSIM}(y, \hat{y}) = \frac{(2\alpha_y\alpha_{\hat{y}} + C_1)(2\beta_{y\hat{y}} + C_2)}{(\alpha_y^2 + \alpha_{\hat{y}}^2 + C_1)(\beta_y^2 + \beta_{\hat{y}}^2 + C_2)} \quad (11)$$

In this formula,  $\alpha_y$  and  $\alpha_{\hat{y}}$  denote the mean values of  $y$  and  $\hat{y}$ , representing their average luminance. The terms  $\beta_y^2$  and  $\beta_{\hat{y}}^2$  are the variances of  $y$  and  $\hat{y}$ , capturing the contrast within each image. The covariance  $\beta_{y\hat{y}}$  reflects the structural similarity between  $y$  and  $\hat{y}$ , and  $C_1$  and  $C_2$  are constants added to stabilize the formula for small  $\alpha$  and  $\beta$ .

## 4 Physically Interpretable World Models

Our physically interpretable world models (PIWMs) use a standard VAE structure as a skeleton. The encoder  $f_{\text{enc}}$  takes the observation  $y_t$  as input and the output  $z_t$  has the same dimension as the state  $x_t$ . A customized dynamical layer  $\phi$  is designed as a sequence predictor to generate predicted state  $z_{t+1}$  at the next moment. Finally, the decoder  $f_{\text{dec}}$  takes the latent representation  $z_{t+1}$  as input to reconstruct the image  $\hat{y}_{t+1}$ . This reconstructed observation serves as the predicted observation for the next moment and is specifically designed as input to the controller to generate an action  $a_{t+1}$ . The generated action  $a_{t+1}$  is applied to the environment to influence the system’s next state, closing the feedback loop. The Fig. 1 shows the overview of our proposed architecture:

1. **Encoder:** Converts high-dimensional observations into physically meaningful latent representations (Section 4.2).
2. **Dynamical Layer:** Predicts the next latent vector based on the current one and the action (Section 4.1).
3. **Decoder:** Reconstructs the observation from the predicted latent vector and feeds it into the controller (Section 4.2).

PIWM is an end-to-end model: all the components of the model are trained together. Its loss function combines the reconstruction loss and the weakly-supervised physical signal. The central challenge in implementing our architecture is giving the latent values a physical meaning while maintaining efficient encoding and high-performance decoding under weak supervision.

### 4.1 Dynamical Layer

Since the system’s dynamics function  $\phi$  operates in a lower-dimensional space, defined as  $\phi(x_t, a_t) = x_{t+1}$ , we introduce a latent representation  $z$ , and  $\dim(z) \geq \dim(x)$ . The first few dimensions of the latent representation

$z' = z[0 : \dim(x)]$  are assigned to represent the physical states corresponding to  $x$ , ensuring consistency between the latent space and the original state space. The latent representation  $z'$  serves as the input to the dynamics function, allowing the model to predict the future latent state. Mathematically, this is expressed as:

$$z'_{t+1} = \phi(z'_t, a_t), \quad (12)$$

where  $\phi$  represents the dynamics function.

This dynamics function forms the core of the *dynamical layer*, a prediction module integrated into our model architecture. While the structure of the dynamics function (i.e., its governing equations) is known, the exact values of its true parameters, denoted as  $\psi^*$ , are unknown. The parameters within this layer are learnable and initialized randomly, enabling the model to approximate  $\psi^*$  during training. For example, in a cart-pole system, the state  $x$  includes variables such as the cart’s position, velocity, and the pole’s angle and angular velocity. By encoding the observation  $y$  into a latent space  $z$ , the model captures the physical relationships among these variables, allowing for an interpretable and physically consistent evolution.

## 4.2 Learning Physically Interpretable Representations with Weak Supervision

The encoder and decoder structures in our model are adapted from the VAE framework [6]. In a standard VAE, the observed data  $y$  is assumed to be generated from an underlying latent variable  $z$  through a conditional probability distribution  $p(y | z)$ . The goal of the standard VAE is to find a compact representation  $z$  that captures essential features in  $y$  while allowing for this data generation. This is achieved by maximizing the probability of observing  $y$  from our training data  $V$ , expressed as the marginal likelihood  $p(y) = \int p(y | z)p(z) dz$ .

However, directly computing  $p(y)$  is generally intractable due to the complexity of integrating over  $z$ . To address this, VAE introduces an approximate posterior distribution  $q(z|y)$ , which represents the probability of latent  $z$  given the data  $y$ . This approximation is parameterized by the encoder network  $f_{\text{enc}}$  and serves as a tractable substitute for the true posterior  $p(z|y)$ . This approximation step is the basis for our approach as well, enabling the encoder to approximate the uncertain physical values (e.g., the positions and angles) implied by an image observation.

In basic VAEs, the latent variable  $z$  is typically constrained by a standard Gaussian prior distribution  $p(z) = \mathcal{N}(0, 1)$ , to regularize the latent space. This technique helps avoid discontinuities and poor-performance “holes” in the latent space around value 0. Unfortunately, it results in  $z$  being an abstract, non-physical representation with values around 0.

In our approach, we change that prior by incorporating weak supervisory signals to make  $z$  more physically meaningful. To achieve this, we utilize available interval constraints from the training data  $V$ , which capture physical ranges or limits. To ensure compatibility with the Gaussian-based KL divergence used in VAE training, we encode the intervals as Gaussian distributions centered within their respective ranges. By aligning the latent representation  $z$  with these distributions, our PIWM makes  $z$  reflect the physical properties of the system, not necessarily close to 0.

VAE models are trained by maximizing a lower bound on  $\log p(y)$ , known as the evidence lower bound (ELBO):

$$\log p(y) \geq \mathbb{E}_{q(z|y)} [\log p(y|z)] - D_{KL}(q(z|y) \parallel \mathcal{N}(0, 1)), \quad (13)$$

where the first term,  $\mathbb{E}_{q(z|y)} [\log p(y|z)]$ , represents the expected log-likelihood of the data  $y$  given the latent variable  $z$ . This term quantifies how well the decoder, which generates  $y$  from  $z$ , reconstructs the input data and is thus related to the reconstruction accuracy. The second term,  $D_{KL}(q(z|y) \parallel \mathcal{N}(0, 1))$ , is the Kullback-Leibler (KL) divergence, defined as

$$D_{KL}(q(z|y) \parallel p(z)) = \int q(z|y) \log \frac{q(z|y)}{p(z)} dz. \quad (14)$$

We extend this objective function to regularize the latent space with the weakly supervised intervals:

$$\log p(y) \geq \mathbb{E}_{q(z|y)} [\log p(y|z)] - D_{KL}(q(z|y) \parallel \mathcal{N}(\mu', \sigma'^2)), \quad (15)$$

where  $\mathcal{N}(\mu', \sigma'^2)$  replaces the prior distribution  $\mathcal{N}(0, 1)$  and represents the Gaussian fit to the weak supervision signal.

The mean  $\mu'$  is set to the center of the given interval,  $\mu'_p = \frac{x_{\text{lo}}^i + x_{\text{up}}^i}{2}$ , and the standard deviation  $\sigma'$  is defined as  $\sigma'_p = \frac{x_{\text{up}}^i - x_{\text{lo}}^i}{6}$ , such that the interval aligns with the  $\pm 3\sigma$  range of a Gaussian distribution, covering approximately 99.73% of the probability mass. For digits non-states representations  $z[\dim(x) : \dim(x) + \dim(z)]$ ,  $\mathcal{N}(0, 1)$  is applied as a prior.

This term encourages  $z$  to align with meaningful ranges, ensuring that the latent space is organized around real physical value ranges rather than an arbitrary standard normal prior.

Our learned representation  $z$  is derived using the reparameterization trick commonly used in VAEs, which allows for gradient-based optimization while preserving the stochastic nature of the model. Specifically, the latent variable  $z$  is computed as:

$$z = f_{enc}(y) = \mu(y) + \sigma(y) \cdot \epsilon, \quad (16)$$

where  $\epsilon \sim \mathcal{N}(0, I)$  is standard Gaussian noise, and  $\mu(y)$  and  $\sigma(y)$  are outputs of the encoder network. Unlike standard VAEs, where the prior distribution is  $\mathcal{N}(0, 1)$ , our approach incorporates a weakly supervised Gaussian prior  $\mathcal{N}(\mu', \sigma'^2)$ . The encoder learns to align  $\mu(y)$  with  $\mu'$  and scales  $\sigma(y)$  to match  $\sigma'$ , ensuring that the latent space respects physical ranges defined by the weak supervision signals. This design enables  $z$  to capture both the expected values and the uncertainty of partially observable physical properties (e.g., positions or angles inferred from low-resolution images).

In practice, a key challenge is to efficiently learn latent representations that are both physically grounded and capable of generalizing across diverse physical ranges defined by weak supervision. To address this, we adopt amortized variational inference [58], where the encoder neural network shares parameters across all data points rather than optimizing separate variational parameters for each instance. By doing so, the encoder leverages common structural patterns within the dataset, ensuring that the learned latent representations  $z$  remain coherent and physically meaningful. This parameter sharing not only reduces computational overhead but also facilitates scaling to larger datasets, resulting in a more robust and adaptable inference process for varied physical scenarios.

The output of the decoder network is then our predicted observation:

$$\hat{y} = f_{dec}(z) \quad (17)$$

The target distribution  $p(z_{t+1})$  is thus modeled as a multivariate Gaussian due to the multi-dimension of the states:

$$p(z_{t+1}) = \mathcal{N}(z_{t+1}; \mu_p, \text{diag}((\sigma_p^i)^2)), \quad (18)$$

where  $\mu_p = [\mu_p^1, \mu_p^2, \dots, \mu_p^d]$  and  $\text{diag}((\sigma_p^i)^2)$  is the diagonal covariance matrix with entries  $(\sigma_p^1)^2, (\sigma_p^2)^2, \dots, (\sigma_p^d)^2$ , each corresponding to one of the  $d$  dimensions of  $z$ .

We add the Cross Entropy loss term to further improve the quality of the reconstructed images by encouraging the model to produce reconstructions closer to the original inputs. The modified VAE loss function, incorporating the dynamical layer and weak supervision, becomes:

$$\begin{aligned} \mathcal{L} &= -\mathbb{E}_{q(z|y)}[\log p(y|z)] \\ &\quad + \lambda_1 \cdot D_{\text{KL}}(q(z_{t+1}|z_t) \parallel p(z_{t+1})) \\ &\quad + \lambda_2 \cdot \mathcal{L}_{\text{CE}}(h(y), h(y_{\text{recon}})) \\ &= -\mathbb{E}_{q(z|y)}[\log p(y|z)] \\ &\quad + \lambda_1 \cdot \sum_z q(z_{t+1}|z_t) \log \frac{q(z_{t+1}|z_t)}{p(z_{t+1})} \\ &\quad - \lambda_2 \cdot \log(h(y_{\text{recon}})_{h(y)}) \end{aligned} \quad (19)$$

Here,  $h(y)$  and  $h(y_{\text{recon}})$  are the actions generated by the controller that generates actions based on real image and reconstructed image.  $h(y_{\text{recon}})_{h(y)}$  represents the probability value assigned by the distribution  $h(y_{\text{recon}})$  to the true action class  $h(y)$ . Our approach learns the unknown parameters within the dynamical layer and the parameter of the encoder-decoder pair, aligning the latent space with representations that are consistent with the system's physical dynamics and making use of weak supervision to capture meaningful physical states across each dimension.

This iterative process continues over the prediction horizon which is  $k$  steps, allowing the model to learn a sequence of latent representations that align with the physical dynamics of the system. The entire training procedure is detailed in Algorithm 1, which describes the process of jointly learning physical representation and dynamics with batch input. First, the training dataset, consisting of sequences of images, actions, and weak state labels, is divided into batches. For each batch, the observations are encoded using the encoder  $f_{enc}$ , and latent variables are sampled. The dynamics model  $\phi$  predicts the latent variables for the next time step based on the current latent state and action. The decoder  $f_{dec}$  reconstructs the observed images, and the reconstruction loss is computed. Additionally, a KL divergence loss is calculated to regularize the latent space. The parameters of the model are updated using the Adam optimizer, with the process repeated for each batch until convergence.

In Algorithm 2 after the training, we present a prediction algorithm that takes any observation  $y$  as input and generates the subsequent  $k$  steps of predictions for both the physically interpretable representations  $z$  and the observations  $y$ .

**Algorithm 1:** Joint Learning of Physical Representation and Dynamics with Batch Input**Input:** Training dataset  $V$  that contains sequences of images, actions, and weak state labels $(y_{1:M}, a_{1:M}, [x_{1:M}^{lo}, x_{1:M}^{up}])$ , batch size  $B$ , controller  $h$ , weights  $\lambda_1, \lambda_2$  and optimizer Adam()**Output:** Well-trained PIWM model  $(f_{enc}, \phi, f_{dec})$  with combined parameters  $\theta$ 

```

1 Initialize parameters  $\theta$  with random values;
2 for  $i \leftarrow 1$  to  $\text{len}(V)/B$  do
3   Sample a batch of  $B$  sequences from  $V$ ;
4   foreach sequence in batch do
5     for  $j \leftarrow 1$  to  $M - 1$  do
6        $(\mu_{z_j}, \sigma_{z_j}^2) = f_{enc}(y_j)$ ; // Encode observations
7        $z_j \sim \mathcal{N}(\mu_{z_j}, \sigma_{z_j}^2)$ ; // Sample latents
8        $z_{j+1} = \phi(z_j, a_j)$ ; // Predict latents
9        $\hat{y}_{j+1} = f_{dec}(z_{j+1})$ ; // Reconstruct image
10       $\mathcal{L}_0 = \frac{1}{D} \sum_{k=1}^D \|\hat{y}_{j+1} - y_{j+1}\|^2$ ; // Reconstruction loss
11       $p \sim \mathcal{N}\left(\frac{x_{t-m:t}^{upk} - x_{t-m:t}^{lo_k}}{2}, \left(\frac{x_{t-m:t}^{lo_i} + x_{t-m:t}^{up_i}}{6}\right)^2\right) = \mathcal{N}(\mu_p, \sigma_p^2)$ ;
12       $q \sim \mathcal{N}(\mu_{z_j}, \sigma_{z_j}^2) = \mathcal{N}(\mu_q, \sigma_q^2)$ ;
13       $\mathcal{L}_1 = \sum_{k=1}^d \left\| \frac{1}{2} \left( \frac{\sigma_p^2}{\sigma_q^2} + \frac{(\mu_q - \mu_p)^2}{\sigma_q^2} - 1 + \ln \frac{\sigma_q^2}{\sigma_p^2} \right) \right\|^2$ ; // KL divergence
14       $\mathcal{L}_2 = \lambda_2 \cdot \mathcal{L}_{CE}(h(\hat{y}_{j+1}), h(y_{j+1}))$ ; // Action loss
15      Update parameters:  $\theta \leftarrow \text{Adam}(\theta, \nabla_{\theta}(\mathcal{L}_0 + \lambda_2 \mathcal{L}_1 + \lambda_2 \mathcal{L}_2))$ ;
16      ; // Update parameters over the batch
17 return  $\theta$ 

```

**Algorithm 2:** PIWM Prediction Algorithm**Input:** Observation  $y_t$  at any time  $t$ , predictor  $\mathcal{P}_{\theta} = (f_{enc}, \phi, f_{dec})$ , the length of state  $d$  and controller  $h$ **Output:** Physical interpretable latent representations  $z_{t:t+k}$ , and predicted observation  $\hat{y}_{t+1:t+k}$ 

```

1  $Z \leftarrow [], \hat{Y} \leftarrow []$ ; // Lists to store predictions
2  $a \leftarrow a_t$ 
3  $(\mu_{z_t}, \sigma_{z_t}^2) = f_{enc}(y_t)$ ; // Encode images
4  $z_t \sim \mathcal{N}(\mu_{z_t}, \sigma_{z_t}^2)$ ; // Sample latents
5  $z'_t \leftarrow z_t[0:d]$ 
6 for  $i \leftarrow t$  to  $t+k$  do
7    $z'_{i+1} = \phi(z'_i, a)$ ; // Predict latents
8    $z_{i+1} \leftarrow [z'_{i+1}, z_i[d:d + \text{len}(z_i)]]$ 
9    $\hat{y}_{i+1} = f_{dec}(z_{i+1})$ ; // Reconstruct images
10   $\hat{Y}.append(\hat{y}_{i+1})$ 
11   $Z.append(z_{i+1})$ 
12   $a \leftarrow h(\hat{y}_{i+1})$ ; // Generate actions
13 return  $Z, \hat{Y}$ ;

```

## 5 Experimental Evaluation

The objective of our experiments is to evaluate the accuracy of the proposed model, focusing specifically on its performance in simulation environments from OpenAI’s gym [59]: the cartpole and lunar lander tasks. First, we assess the effectiveness of the weakly supervised learning mechanism in capturing physically meaningful representations within the latent space and aligning them with actual physical states. Second, we evaluate prediction accuracy by comparing the predicted future states with true values under varying time horizons and levels of noise in the supervision signal. These evaluations are done in comparison with baseline models. Finally, we analyze the dynamical layer’s contribution to the accuracy and physicality of sequence prediction.

## 5.1 Experiment Setup

We experiment on two well-known control tasks — lunar lander and cart pole [59] — to assess the proposed framework’s suitability for vision-based dynamical systems. In the cart pole, the task is to balance a pole on a moving cart by applying forces to the cart in one of two directions. This task has a four-dimensional state space (position, velocity, angle, and angular velocity) and a binary discrete action space (pull left or right), allowing only left or right movements. The lunar lander’s task is to guide a lander to a safe landing. This task has an eight-dimensional state space: horizontal and vertical positions, velocities, angle, angular velocity, and information about the lander’s contact with the ground. It also has a four-dimensional action space, allowing for finer control by activating the main engine and side thrusters. The lunar lander task is more complex than the cart pole, requiring precise control and handling of multiple variables, testing the model’s ability to capture complex relationships in both state and action spaces. There are 4 parameters of dynamics in a cart pole: the mass of the cart and pole, the length of the pole, and the force implemented on the cart. For the lunar lander, there are 2 parameters: the power of the main engine which controls the landing speed, and the power of the side engine which is responsible for adjusting the landing directions.

For each task, training, validation, and test data were collected from three different controllers that were trained with reinforcement learning (DQN) algorithm, ensuring diversity in the collected trajectories. For each task,  $N = 40,000$ , indicating the total number of trajectories collected, and  $M = 50$ , representing the number of time steps in each trajectory. The maximum of the prediction horizon is set to  $k = 30$ . 20,000 trajectories are collected for both validation and test datasets.

The encoder and decoder use basic convolutional and deconvolutional architectures, respectively. Baseline comparisons include VAE+LSTM and  $\beta$ -VAE+LSTM ( $\beta=4$ ) models using the same loss functions, as well as a non-trainable, true dynamical system for performance benchmarking. To test the effect of weak supervision, we applied interval constraints with lengths covering 2.5%, 5%, and 10% of the state space. These intervals were either centered around the true values or randomly shifted (noted as “shift” later in the result tables) so that the true values fell within the interval without necessarily being centered. This setup allowed us to examine how different levels of weak supervision, both with and without exact centering on the true values.

Another set of ablation experiments was conducted to assess how precise supervision using true state values impacts prediction accuracy and physical interpretability. In these experiments, the proposed model and baseline models (VAE&LSTM and  $\beta$ -VAE&LSTM) were trained using the loss function described in Alg 1, with true values as direct supervision signals. This setup provides ideal benchmarks for comparing the effectiveness of weak versus full supervision, allowing us to evaluate how much accuracy and physical alignment may be compromised under weak supervision conditions. These ablation experiments also allow us to investigate the effects of different loss function designs on model performance. While MSE enforces strict alignment with true values, weak supervision employs interval constraints, which allow some flexibility. This distinction reveals how loss functions shape model behavior.

All models are trained with a batch size of 32 and an initial learning rate of 0.001, using the Adam optimizer. Training was conducted for 200 epochs, with the learning rate set to decay when the loss plateaued. All experiments were performed on an NVidia A100 GPU, which provided the computational power needed for handling high-dimensional inputs and complex dynamical simulations.

## 5.2 Results

### 5.3 Results Analysis

Figure 2 shows the prediction performance on the cart-pole environment. It is evident that our PIWM outperforms both the VAE-LSTM and the *beta*-VAE-based world models in terms of predicting both the cart position and the pole angle. The leftmost column in the figure corresponds to a model variant trained with a mean-squared error (MSE) loss function as a baseline ablation.

As the interval length increases, we observe a general trend of rising prediction errors. This effect becomes more pronounced as the prediction horizon extends, reflecting the increasing difficulty of long-term forecasting. Notably, when the interval length is set to 10%, the PIWM variant that incorporates an action loss surpasses the PIWM variant without action loss. This result suggests that including action-related information can further enhance predictive accuracy, especially under conditions of weaker supervisory signals.

From the static data reported in Table 1, we observe that the encoding of states from images produces error values for all models that are smaller than the predefined interval widths. This finding underscores the effectiveness of combining weak supervision signals with underlying dynamics to learn interpretable representations. It indicates that the latent

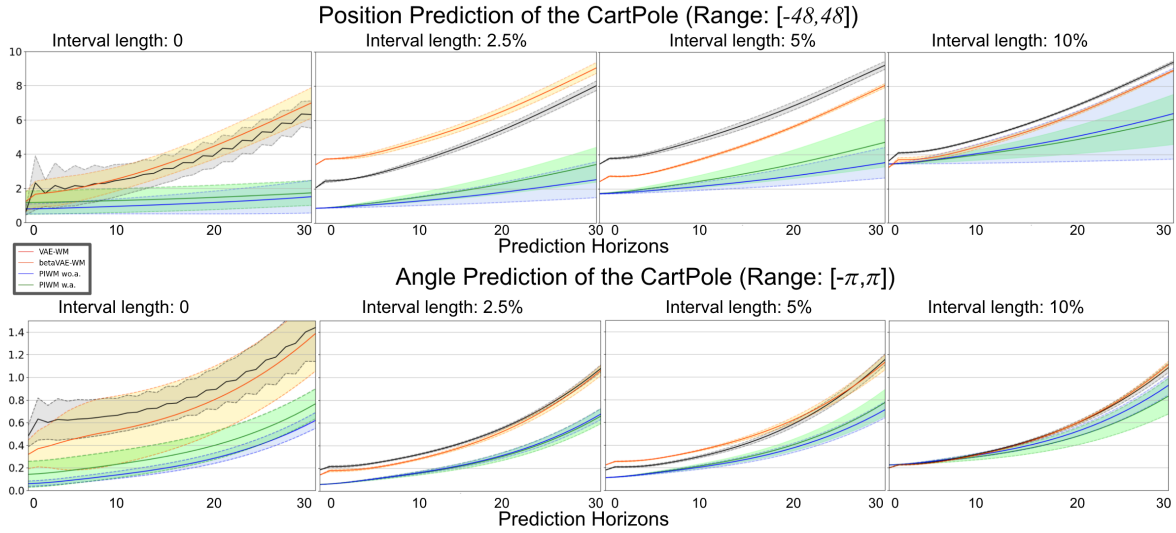


Figure 2: State prediction performance for the *cart pole*: the mean absolute error (MAE) for the cart’s position and the pole’s angle. The 0 interval length indicates the use of additional data.

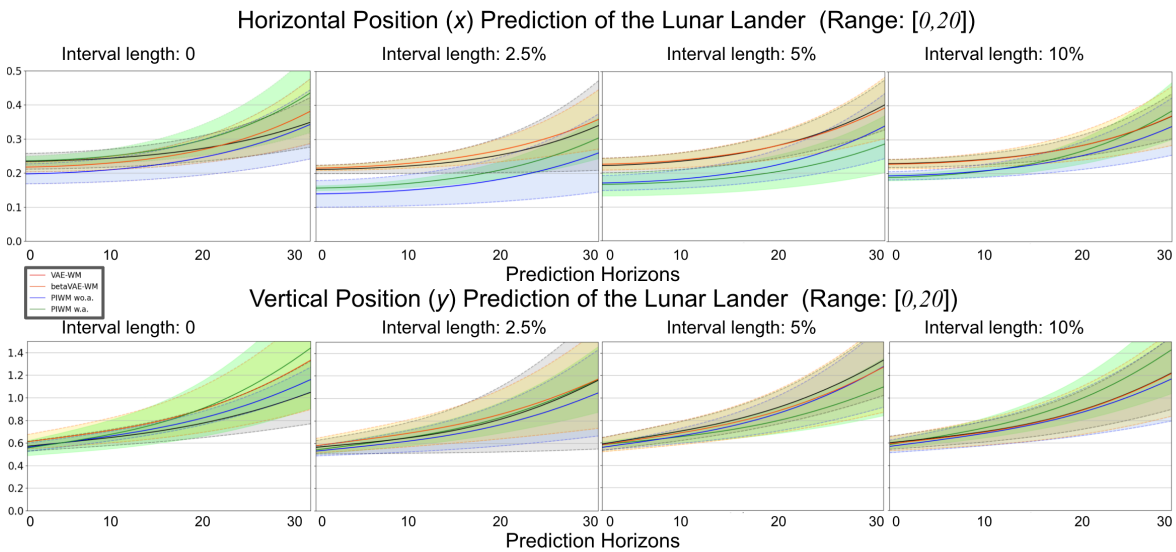


Figure 3: State prediction performance for the *lunar lander*: the mean absolute error (MAE) for the lander’s horizontal position and the vertical position. The 0 interval length indicates the use of additional data.

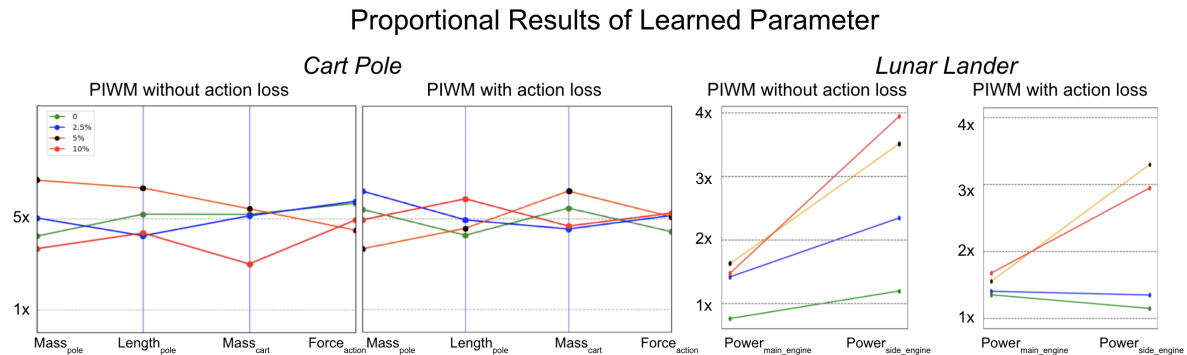


Figure 4: Learned parameter of *cart pole* (left two) and *lunar lander* (right two).

Table 1: Static Results Cart Pole: Interpretable Encoding Error and Reconstruction Quality

Model	Interval Length	x Error	Angle Error	SSIM	MSE
Real	0	0	0	1	0
VAE-WM	0	<b>0.564 ± 0.141</b>	0.479 ± 0.094	0.991 ± 0.004	0.0002 ± 0.0000
betaVAE WM	0	0.863 ± 0.251	0.404 ± 0.030	0.989 ± 0.007	0.0004 ± 0.0001
PIWM w.a	0	1.165 ± 0.684	0.143 ± 0.115	0.994 ± 0.004	0.0002 ± 0.0001
PIWM wo.a	0	0.791 ± 0.289	<b>0.060 ± 0.023</b>	0.981 ± 0.012	0.0003 ± 0.0001
VAE-WM	2.5	2.051 ± 0.359	0.186 ± 0.025	0.995 ± 0.001	0.0002 ± 0.0000
betaVAE WM	2.5	3.402 ± 0.488	0.141 ± 0.046	0.993 ± 0.000	0.0004 ± 0.0000
PIWM w.a	2.5	<b>0.861 ± 0.008</b>	0.058 ± 0.002	0.977 ± 0.012	0.0003 ± 0.0001
PIWM wo.a	2.5	0.865 ± 0.016	<b>0.058 ± 0.001</b>	0.992 ± 0.004	0.0002 ± 0.0000
VAE-WM	5	3.443 ± 0.390	0.179 ± 0.014	0.992 ± 0.004	0.0003 ± 0.0000
betaVAE WM	5	2.413 ± 0.509	0.224 ± 0.060	0.992 ± 0.001	0.0004 ± 0.0000
PIWM w.a	5	1.728 ± 0.020	<b>0.113 ± 0.001</b>	0.965 ± 0.038	0.0009 ± 0.0014
PIWM wo.a	5	<b>1.710 ± 0.018</b>	0.113 ± 0.001	0.993 ± 0.007	0.0002 ± 0.0001
VAE-WM	10	3.614 ± 0.486	<b>0.199 ± 0.008</b>	0.995 ± 0.000	0.0002 ± 0.0000
betaVAE WM	10	<b>3.235 ± 0.366</b>	0.199 ± 0.015	0.992 ± 0.001	0.0004 ± 0.0000
PIWM w.a	10	3.438 ± 0.049	0.225 ± 0.003	0.969 ± 0.014	0.0003 ± 0.0001
PIWM wo.a	10	3.443 ± 0.030	0.225 ± 0.003	0.993 ± 0.006	0.0002 ± 0.0001

Table 2: Static Results Lunar Lander: Interpretable Encoding Error and Reconstruction Quality

Model	Interval Length	x Error	y Error	SSIM	MSE
Real	0	0	0	1	0
VAE-WM	0	0.234 ± 0.023	0.559 ± 0.038	0.956 ± 0.007	0.0007 ± 0.0013
betaVAE WM	0	0.209 ± 0.014	0.596 ± 0.057	0.968 ± 0.011	0.0006 ± 0.0013
PIWM w.a	0	0.235 ± 0.013	<b>0.537 ± 0.026</b>	0.979 ± 0.012	0.0003 ± 0.0011
PIWM wo.a	0	<b>0.197 ± 0.029</b>	0.546 ± 0.037	0.995 ± 0.002	0.0004 ± 0.0011
VAE-WM	2.5	0.211 ± 0.012	0.554 ± 0.050	0.970 ± 0.007	0.0004 ± 0.0011
betaVAE WM	2.5	0.156 ± 0.011	0.564 ± 0.058	0.975 ± 0.011	0.0006 ± 0.0011
PIWM w.a	2.5	0.217 ± 0.007	0.527 ± 0.030	0.972 ± 0.009	0.0008 ± 0.0010
PIWM wo.a	2.5	<b>0.139 ± 0.039</b>	<b>0.519 ± 0.035</b>	0.965 ± 0.005	0.0006 ± 0.0012
VAE-WM	5	0.221 ± 0.021	0.589 ± 0.057	0.941 ± 0.010	0.0003 ± 0.0012
betaVAE WM	5	0.225 ± 0.017	0.582 ± 0.062	0.949 ± 0.001	0.0005 ± 0.0009
PIWM w.a	5	<b>0.166 ± 0.034</b>	0.572 ± 0.021	0.980 ± 0.015	0.0004 ± 0.0008
PIWM wo.a	5	0.170 ± 0.022	<b>0.543 ± 0.019</b>	0.963 ± 0.003	0.0012 ± 0.0008
VAE-WM	10	0.229 ± 0.011	0.601 ± 0.058	0.972 ± 0.010	0.0009 ± 0.0011
betaVAE WM	10	0.227 ± 0.013	0.591 ± 0.061	0.978 ± 0.012	0.0019 ± 0.0013
PIWM w.a	10	<b>0.188 ± 0.009</b>	0.566 ± 0.029	0.980 ± 0.011	0.0009 ± 0.0015
PIWM wo.a	10	0.193 ± 0.012	<b>0.553 ± 0.049</b>	0.972 ± 0.014	0.0004 ± 0.0012

states not only capture essential system properties but also remain well-aligned with physical intervals informed by weak constraints.

Moreover, the MSE and SSIM metrics appear comparable across all evaluated models, suggesting that each approach excels at reconstructing observations. Such high-quality reconstructions are consistent with the role of a world model, which should reliably generate plausible next-step observations based on current inputs. In other words, all methods successfully fulfill the fundamental requirement of producing coherent predictions that accurately reflect the underlying system dynamics.

Figure 4 illustrates the learned parameters of the dynamical system for the cart-pole environment. Empirical observation reveals that the four parameters discovered by our model maintain a consistent proportionality with the ground-truth parameters, approximately a factor of five greater than their true values. In this particular system, scaling both mass and force by the same factor does not alter the resulting accelerations, contributing to the observed parameter scaling. However, the learned pole length diverges from the ground-truth value, introducing a source of error in the predictions.

This discrepancy indicates that while the model can approximate the underlying dynamics with proportional accuracy, certain parameters remain challenging to estimate precisely and may require additional constraints or supervision.

Figure 3 presents the state prediction results for the Lunar Lander environment. Similar to the cart-pole scenario, we observe that prediction errors increase as the task complexity and interval length grow. Notably, our PIWM model demonstrates a substantial advantage during shorter prediction horizons—for instance, within the first 20 steps—outperforming the compared ablation models.

Table 2 shows the static results and indicates that the PIWM consistently encodes more meaningful representations than the other variants. Both the MSE and SSIM metrics are within excellent, reasonable ranges, ensuring that the model effectively reconstructs observations consistent with the underlying dynamics.

For longer-term predictions, the complexity of the Lunar Lander environment’s varied terrains adds to the challenge of accurate encoding and decoding. Nevertheless, the learned dynamic parameters displayed on the right side of Figure 4 confirm that the PIWM captures essential properties of the environment. Specifically, the learned main engine power closely approximates the true value, which correlates well with improved accuracy in the vertical (y-axis) position prediction. Compared to standard VAE or  $\beta$ -VAE models, our PIWM achieves more precise parameter estimates. Moreover, when augmented with the action loss, the PIWM excels in learning the side engine power, further enhancing its interpretability and predictive performance.

In summary, the PIWM not only attains superior predictive accuracy and stable reconstructions in the Lunar Lander setting but also demonstrates an enhanced ability to learn physically meaningful parameters of the underlying dynamical system.

## 6 Discussion

Our model demonstrates clear advantages in both short-term and long-term prediction tasks, particularly with weak supervision or known parameters. In the cart pole and lunar lander experiments, PIWM consistently outperforms baseline models, achieving strong physical consistency and interpretability even under minimal supervision (e.g., 2.5%). This capability suggests PIWM’s suitability for applications where only partial state information is available, as it aligns learned representations closely with true physical states.

The PIWM’s strength lies in capturing complex dynamics with minimal supervision, making it effective for high-dimensional tasks requiring stable, accurate predictions. Compared to VAE+LSTM and  $\beta$ -VAE+LSTM models, PIWM shows robustness to limited labeled data, which is beneficial in settings where precise labeling is challenging or costly. However, when the interval constraints become wider (e.g., 10%), prediction accuracy shows a slight decline. As prediction horizons increase, maintaining accuracy becomes increasingly difficult, especially in highly dynamic environments.

Future work could enhance PIWM by incorporating finer-grained physical constraints, adaptive supervision, or varying learning rates for extended prediction horizons. Additionally, leveraging invariances in physical systems — such as symmetries in motion dynamics or conservation laws — could further improve the model’s robustness and generalizability. Such enhancements would broaden PIWM’s applicability across diverse physical systems, enabling it to better handle tasks with varying levels of observability and supervision.

In summary, PIWM effectively encodes physically meaningful representations and maintains predictive accuracy across tasks — a step towards reliable complex CPS where both interpretability and predictive reliability are critical.

## Acknowledgments

The authors would like to thank Vedansh Maheshwari for his help in exploring the baseline approaches and Mrinall Umasudhan for programming the tools to visualize latent spaces. This research is supported in part by the NSF Grant CCF-2403616. Any opinions, findings, conclusions, or recommendations expressed in this material are those of the authors and do not necessarily reflect the views of the National Science Foundation (NSF) or the United States Government.

## References

- [1] Yong Yu, Xiaosheng Si, Changhua Hu, and Jianxun Zhang. A review of recurrent neural networks: Lstm cells and network architectures. *Neural computation*, 31(7):1235–1270, 2019.

- [2] Junyoung Chung, Caglar Gulcehre, KyungHyun Cho, and Yoshua Bengio. Empirical evaluation of gated recurrent neural networks on sequence modeling. *arXiv preprint arXiv:1412.3555*, 2014.
- [3] Shengze Cai, Zhiping Mao, Zhicheng Wang, Minglang Yin, and George Em Karniadakis. Physics-informed neural networks (pinns) for fluid mechanics: A review. *Acta Mechanica Sinica*, 37(12):1727–1738, 2021.
- [4] Ricky TQ Chen, Yulia Rubanova, Jesse Bettencourt, and David K Duvenaud. Neural ordinary differential equations. *Advances in neural information processing systems*, 31, 2018.
- [5] Xingjian Shi, Zhourong Chen, Hao Wang, Dit-Yan Yeung, Wai-Kin Wong, and Wang-chun Woo. Convolutional lstm network: A machine learning approach for precipitation nowcasting. *Advances in neural information processing systems*, 28, 2015.
- [6] Diederik P Kingma. Auto-encoding variational bayes. *arXiv preprint arXiv:1312.6114*, 2013.
- [7] David Ha and Jürgen Schmidhuber. World models. *arXiv preprint arXiv:1803.10122*, 2018.
- [8] Zhenjiang Mao, Carson Sobolewski, and Ivan Ruchkin. How safe am i given what i see? calibrated prediction of safety chances for image-controlled autonomy. In *6th Annual Learning for Dynamics & Control Conference*, pages 1370–1387. PMLR, 2024.
- [9] Vincent Micheli, Eloi Alonso, and François Fleuret. Transformers are sample-efficient world models. *arXiv preprint arXiv:2209.00588*, 2022.
- [10] Osman Hasan and Sofiene Tahar. Formal verification methods. In *Encyclopedia of Information Science and Technology, Third Edition*, pages 7162–7170. IGI global, 2015.
- [11] Masaki Waga, Ezequiel Castellano, Sasinee Pruekprasert, Stefan Klikovits, Toru Takisaka, and Ichiro Hasuo. Dynamic shielding for reinforcement learning in black-box environments. In *International Symposium on Automated Technology for Verification and Analysis*, pages 25–41. Springer, 2022.
- [12] Mengyue Yang, Furui Liu, Zhitang Chen, Xinwei Shen, Jianye Hao, and Jun Wang. Causalvae: Disentangled representation learning via neural structural causal models. In *Proceedings of the IEEE/CVF conference on computer vision and pattern recognition*, pages 9593–9602, 2021.
- [13] Ian Goodfellow, Jean Pouget-Abadie, Mehdi Mirza, Bing Xu, David Warde-Farley, Sherjil Ozair, Aaron Courville, and Yoshua Bengio. Generative adversarial networks. *Communications of the ACM*, 63(11):139–144, 2020.
- [14] Johannes Ballé, Valero Laparra, and Eero P Simoncelli. End-to-end optimized image compression. *arXiv preprint arXiv:1611.01704*, 2016.
- [15] Junyuan Xie, Ross Girshick, and Ali Farhadi. Unsupervised deep embedding for clustering analysis. In *International conference on machine learning*, pages 478–487. PMLR, 2016.
- [16] Yann LeCun, Yoshua Bengio, and Geoffrey Hinton. Deep learning. *nature*, 521(7553):436–444, 2015.
- [17] Zhenjiang Mao, Dong-You Jhong, Ao Wang, and Ivan Ruchkin. Language-enhanced latent representations for out-of-distribution detection in autonomous driving. *Robot Trust for Symbiotic Societies Workshop at IEEE ICRA*, 2024.
- [18] Jishnu Mukhoti, Andreas Kirsch, Joost van Amersfoort, Philip HS Torr, and Yarin Gal. Deep deterministic uncertainty: A new simple baseline. In *Proceedings of the IEEE/CVF Conference on Computer Vision and Pattern Recognition*, pages 24384–24394, 2023.
- [19] Leon A Gatys, Alexander S Ecker, and Matthias Bethge. Image style transfer using convolutional neural networks. In *Proceedings of the IEEE conference on computer vision and pattern recognition*, pages 2414–2423, 2016.
- [20] Irina Higgins, Loic Matthey, Arka Pal, Christopher P Burgess, Xavier Glorot, Matthew M Botvinick, Shakir Mohamed, and Alexander Lerchner. beta-vae: Learning basic visual concepts with a constrained variational framework. *ICLR (Poster)*, 3, 2017.
- [21] Boyuan Chen, Kuang Huang, Sunand Raghupathi, Ishaan Chandratreya, Qiang Du, and Hod Lipson. Automated discovery of fundamental variables hidden in experimental data. *Nature Computational Science*, 2(7):433–442, 2022.
- [22] Bernhard Schölkopf, Francesco Locatello, Stefan Bauer, Nan Rosemary Ke, Nal Kalchbrenner, Anirudh Goyal, and Yoshua Bengio. Toward causal representation learning. *Proceedings of the IEEE*, 109(5):612–634, 2021.
- [23] Dylan Sam, Rattana Pukdee, Daniel P Jeong, Yewon Byun, and J Zico Kolter. Bayesian neural networks with domain knowledge priors. *arXiv preprint arXiv:2402.13410*, 2024.
- [24] Richard S Sutton, Doina Precup, and Satinder Singh. Between mdps and semi-mdps: A framework for temporal abstraction in reinforcement learning. *Artificial intelligence*, 112(1-2):181–211, 1999.

- [25] Amy Zhang, Clare Lyle, Shagun Sodhani, Angelos Filos, Marta Kwiatkowska, Joelle Pineau, Yarin Gal, and Doina Precup. Invariant causal prediction for block mdps. In *International Conference on Machine Learning*, pages 11214–11224. PMLR, 2020.
- [26] Xiang Fu, Ge Yang, Pulkit Agrawal, and Tommi Jaakkola. Learning task informed abstractions. In *International Conference on Machine Learning*, pages 3480–3491. PMLR, 2021.
- [27] Chuan Wen, Xingyu Lin, John So, Kai Chen, Qi Dou, Yang Gao, and Pieter Abbeel. Any-point trajectory modeling for policy learning. *arXiv preprint arXiv:2401.00025*, 2023.
- [28] George Konidaris, Leslie Pack Kaelbling, and Tomas Lozano-Perez. From skills to symbols: Learning symbolic representations for abstract high-level planning. *Journal of Artificial Intelligence Research*, 61:215–289, 2018.
- [29] Andi Peng, Mycal Tucker, Eoin Kenny, Noga Zaslavsky, Pulkit Agrawal, and Julie A Shah. Human-guided complexity-controlled abstractions. *Advances in Neural Information Processing Systems*, 36, 2024.
- [30] Andi Peng, Ilya Sucholutsky, Belinda Z. Li, Theodore R. Sumers, Thomas L. Griffiths, Jacob Andreas, and Julie A. Shah. Learning with language-guided state abstractions, 2024.
- [31] Danijar Hafner, Timothy Lillicrap, Ian Fischer, Ruben Villegas, David Ha, Honglak Lee, and James Davidson. Learning latent dynamics for planning from pixels. In *International conference on machine learning*, pages 2555–2565. PMLR, 2019.
- [32] Philipp Wu, Alejandro Escontrela, Danijar Hafner, Pieter Abbeel, and Ken Goldberg. Daydreamer: World models for physical robot learning. In *Conference on robot learning*, pages 2226–2240. PMLR, 2023.
- [33] Danijar Hafner, Timothy Lillicrap, Mohammad Norouzi, and Jimmy Ba. Mastering atari with discrete world models. *arXiv preprint arXiv:2010.02193*, 2020.
- [34] Renukanandan Tumu, Lars Lindemann, Truong Nghiem, and Rahul Mangharam. Physics constrained motion prediction with uncertainty quantification. In *2023 IEEE Intelligent Vehicles Symposium (IV)*, pages 1–8. IEEE, 2023.
- [35] Henggang Cui, Thi Nguyen, Fang-Chieh Chou, Tsung-Han Lin, Jeff Schneider, David Bradley, and Nemanja Djuric. Deep kinematic models for kinematically feasible vehicle trajectory predictions. In *2020 IEEE International Conference on Robotics and Automation (ICRA)*, pages 10563–10569. IEEE, 2020.
- [36] Meiyi Ma, Ji Gao, Lu Feng, and John Stankovic. Stlnet: Signal temporal logic enforced multivariate recurrent neural networks. *Advances in Neural Information Processing Systems*, 33:14604–14614, 2020.
- [37] Alexandre Alahi, Kratarth Goel, Vignesh Ramanathan, Alexandre Robicquet, Li Fei-Fei, and Silvio Savarese. Social lstm: Human trajectory prediction in crowded spaces. In *Proceedings of the IEEE conference on computer vision and pattern recognition*, pages 961–971, 2016.
- [38] Agrim Gupta, Justin Johnson, Li Fei-Fei, Silvio Savarese, and Alexandre Alahi. Social gan: Socially acceptable trajectories with generative adversarial networks. In *Proceedings of the IEEE conference on computer vision and pattern recognition*, pages 2255–2264, 2018.
- [39] Song Wen, Hao Wang, and Dimitris Metaxas. Social ode: Multi-agent trajectory forecasting with neural ordinary differential equations. In *European Conference on Computer Vision*, pages 217–233. Springer, 2022.
- [40] Kaustubh Sridhar, Souradeep Dutta, James Weimer, and Insup Lee. Guaranteed conformance of neurosymbolic models to natural constraints. In *Learning for Dynamics and Control Conference*, pages 76–89. PMLR, 2023.
- [41] Franck Djeumou, Cyrus Neary, and Ufuk Topcu. How to learn and generalize from three minutes of data: Physics-constrained and uncertainty-aware neural stochastic differential equations. *arXiv preprint arXiv:2306.06335*, 2023.
- [42] Weiheng Zhong and Hadi Meidani. Pi-vae: Physics-informed variational auto-encoder for stochastic differential equations. *Computer Methods in Applied Mechanics and Engineering*, 403:115664, 2023.
- [43] Samer Ammoun and Fawzi Nashashibi. Real time trajectory prediction for collision risk estimation between vehicles. In *2009 IEEE 5Th international conference on intelligent computer communication and processing*, pages 417–422. IEEE, 2009.
- [44] David Fridovich-Keil, Andrea Bajcsy, Jaime F Fisac, Sylvia L Herbert, Steven Wang, Anca D Dragan, and Claire J Tomlin. Confidence-aware motion prediction for real-time collision avoidance1. *The International Journal of Robotics Research*, 39(2-3):250–265, 2020.
- [45] Anjian Li, Liting Sun, Wei Zhan, Masayoshi Tomizuka, and Mo Chen. Prediction-based reachability for collision avoidance in autonomous driving. In *2021 IEEE International Conference on Robotics and Automation (ICRA)*, pages 7908–7914. IEEE, 2021.

- [46] Kensuke Nakamura and Somil Bansal. Online update of safety assurances using confidence-based predictions. In *2023 IEEE International Conference on Robotics and Automation (ICRA)*, pages 12765–12771. IEEE, 2023.
- [47] Aastha Acharya, Rebecca Russell, and Nisar R Ahmed. Learning to forecast aleatoric and epistemic uncertainties over long horizon trajectories. In *2023 IEEE International Conference on Robotics and Automation (ICRA)*, pages 12751–12757. IEEE, 2023.
- [48] Tim Salzmann, Boris Ivanovic, Punarjay Chakravarty, and Marco Pavone. Trajectron++: Dynamically-feasible trajectory forecasting with heterogeneous data. In *Computer Vision—ECCV 2020: 16th European Conference, Glasgow, UK, August 23–28, 2020, Proceedings, Part XVIII 16*, pages 683–700. Springer, 2020.
- [49] Ivan Ruchkin, Matthew Cleaveland, Radoslav Ivanov, Pengyuan Lu, Taylor Carpenter, Oleg Sokolsky, and Insup Lee. Confidence composition for monitors of verification assumptions. In *2022 ACM/IEEE 13th International Conference on Cyber-Physical Systems (ICCPs)*, pages 1–12. IEEE, 2022.
- [50] Lars Lindemann, Xin Qin, Jyotirmoy V Deshmukh, and George J Pappas. Conformal prediction for stl runtime verification. In *Proceedings of the ACM/IEEE 14th International Conference on Cyber-Physical Systems (with CPS-IoT Week 2023)*, pages 142–153, 2023.
- [51] Anish Muthali, Haotian Shen, Sampada Deglurkar, Michael H Lim, Rebecca Roelofs, Aleksandra Faust, and Claire Tomlin. Multi-agent reachability calibration with conformal prediction. In *2023 62nd IEEE Conference on Decision and Control (CDC)*, pages 6596–6603. IEEE, 2023.
- [52] Masha Itkina and Mykel Kochenderfer. Interpretable self-aware neural networks for robust trajectory prediction. In *Conference on Robot Learning*, pages 606–617. PMLR, 2023.
- [53] Kai-Chieh Hsu, Karen Leung, Yuxiao Chen, Jaime F Fisac, and Marco Pavone. Interpretable trajectory prediction for autonomous vehicles via counterfactual responsibility. In *2023 IEEE/RSJ International Conference on Intelligent Robots and Systems (IROS)*, pages 5918–5925. IEEE, 2023.
- [54] Ahmed Hussein, Mohamed Medhat Gaber, Eyad Elyan, and Chrisina Jayne. Imitation learning: A survey of learning methods. *ACM Computing Surveys (CSUR)*, 50(2):1–35, 2017.
- [55] Leslie Pack Kaelbling, Michael L Littman, and Andrew W Moore. Reinforcement learning: A survey. *Journal of artificial intelligence research*, 4:237–285, 1996.
- [56] Volodymyr Mnih, Koray Kavukcuoglu, David Silver, Andrei A Rusu, Joel Veness, Marc G Bellemare, Alex Graves, Martin Riedmiller, Andreas K Fidjeland, Georg Ostrovski, et al. Human-level control through deep reinforcement learning. *nature*, 518(7540):529–533, 2015.
- [57] TP Lillicrap. Continuous control with deep reinforcement learning. *arXiv preprint arXiv:1509.02971*, 2015.
- [58] Samuel Gershman and Noah Goodman. Amortized inference in probabilistic reasoning. In *Proceedings of the annual meeting of the cognitive science society*, volume 36, 2014.
- [59] Greg Brockman, Vicki Cheung, Ludwig Pettersson, Jonas Schneider, John Schulman, Jie Tang, and Wojciech Zaremba. Openai gym, 2016.